

Mesoscale modelling of polyelectrolyte electrophoresis

Kai Grass^a and Christian Holm^{a,b,c}

^a Frankfurt Institute for Advanced Studies, Goethe University,
Ruth-Moufang-Str. 1, 60438 Frankfurt/Main, Germany.

E-mail: grass@fias.uni-frankfurt.de

^b Max-Planck-Institut für Polymerforschung,
Ackermannweg 10, 55128 Mainz, Germany.

^c Institute for Computational Physics, University of Stuttgart,
Pfaffenwaldring 27, 70569 Stuttgart,
Germany.

E-mail: holm@icp.uni-stuttgart.de

October 28, 2018

The electrophoretic behaviour of flexible polyelectrolyte chains ranging from single monomers up to long fragments of hundred repeat units is studied by a mesoscopic simulation approach. Abstracting from the atomistic details of the polyelectrolyte and the fluid, a coarse-grained molecular dynamics model connected to a mesoscopic fluid described by the Lattice Boltzmann approach is used to investigate free-solution electrophoresis. Our study demonstrates the importance of hydrodynamic interactions for the electrophoretic motion of polyelectrolytes and quantifies the influence of surrounding ions. The length-dependence of the electrophoretic mobility can be understood by evaluating the scaling behavior of the effective charge and the effective friction. The perfect agreement of our results with experimental measurements shows that all chemical details and fluid structure can be safely neglected, and a suitable coarse-grained approach can yield an accurate description of the physics of the problem, provided that electrostatic and hydrodynamic interactions between all entities in the system, *i.e.*, the polyelectrolyte, dissociated counterions, additional salt and the solvent, are properly accounted for. Our model is able to bridge the single molecule regime of a few nm up to macromolecules with contour lengths of more than 100 nm, a length scale that is currently not accessible to atomistic simulations.

1 Introduction

Nowadays, electrophoresis methods are widely used to separate biomolecules [1, 2] such as peptides, proteins, DNA, as well as synthetic polymers [3, 4]. In order to be able to improve the processes involved in current electrophoretic separation methods it is a prerequisite to gain a thorough understanding of the behaviour of polyelectrolytes

(PEs) in an externally applied electric field. Several theories [5, 6, 7, 8] have been developed to describe PE electrophoresis and successfully described qualitatively the experimentally observed behaviour of various PEs under bulk conditions. However, the mobility of small oligomeric PEs showed under low salt conditions a non-monotonic behaviour that current theories had not been able to explain.

In a recent publication [9], we employed a mesoscopic coarse-grained model using molecular dynamics simulations in connection with a Lattice-Boltzmann (LB) algorithm to extend the theoretical understanding on a more detailed level, and in particular, we intended to investigate the role of hydrodynamic interactions in these systems. Our results were able to match the free-solution electrophoretic mobility μ of short polyelectrolyte chains, here polystyrene sulfonate (PSS), as a function of the number of repeat units N with quantitative agreement to experiments as shown in Figure 4. Since the three data sets have different solvent viscosities the mobility is normalized by the corresponding constant mobility for long chains, the so-called free-draining mobility, μ_{FD} . The electrophoretic mobility increases for short oligomers, reaches a maximum for intermediate degrees of polymerization, and slowly decreases towards a plateau value for long chains. To understand this observation, the hydrodynamic interactions were investigated in detail and we found that they are actually the major driving force for the length dependent mobility for short and intermediate chain lengths. The constant mobility for long chains can be attributed to an effective screening of hydrodynamic interactions, which leads to the so-called free-draining behavior. The inset in Figure 4 shows a comparison to a coarse-grained simulation that neglects hydrodynamic interactions. This leads to a qualitatively completely different behavior, showing a monotonically decreasing mobility. Agreement to the experimentally observed behaviour is only achieved as long as hydrodynamic interactions are included correctly as has been shown in detail in our previous investigations [10, 11].

In this article, we will extend our work by studying the electrophoresis of generic flexible polyelectrolyte chains ranging from single monomers to long fragments of hundred repeat units. Abstracting from the atomistic details of the polyelectrolyte and the fluid, a coarse-grained molecular dynamics model connected to a mesoscopic fluid described by the Lattice Boltzmann approach is used to investigate the free-solution behavior under varying salt concentration.

In the next section we will introduce the employed simulation model. In Section 3, the main results of this study are presented and discussed. We conclude with final remarks in Section 4.

2 Model

We employ molecular dynamics (MD) simulations using the ESPResSo package [12] to study the behaviour of linear polyelectrolytes (PE) of different lengths. The PEs are modelled by a totally flexible bead-spring model. The monomers are connected to each other by finitely extensible nonlinear elastic (FENE) bonds [13]

$$U_{\text{FENE}}(r) = \frac{1}{2}kR^2 \ln \left(1 - \left(\frac{r}{R} \right)^2 \right),$$

with stiffness $k = 30\epsilon_0$, and maximum extension $R = 1.5\sigma_0$, where r is the distance between the interacting monomers. Additionally, a truncated Lennard-Jones or WCA

potential [14]

$$U_{\text{LJ}}(r < r_c) = \epsilon_0 \left(\left(\frac{\sigma_0}{r} \right)^{12} - \left(\frac{\sigma_0}{r} \right)^6 + \frac{1}{4} \right),$$

is used for excluded volume interactions between all monomers. A cutoff value of $r_c = \sqrt[6]{2}\sigma_0$ ensures a purely repulsive potential. All dissociated counterions and additional salt ions are modelled by appropriately charged spheres using the same WCA potential.

Here, ϵ_0 and σ_0 define the energy and length scale of the simulations. We use $\epsilon_0 = k_{\text{B}}T$, i.e. the energy of the system is expressed in terms of the thermal energy. The length scale σ_0 defines the size of the monomers and the dimension of the system. For this study, σ_0 is chosen to be 4 Å. Different polyelectrolytes can be mapped by changing σ_0 . Unless mentioned otherwise, all observables are expressed in reduced simulation units, and we will not use σ_0 and ϵ_0 explicitly from now on.

The chain length is varied from $N = 1$ to $N = 128$ and all chain monomers carry a negative electric charge $q = -1e_0$, where e_0 is the elementary charge. For charge neutrality, N monovalent counterions of charge $+1e_0$ are added. Additional monovalent salt is added to the simulation, corresponding to concentrations between $c_s = 0$ mM and $c_s = 160$ mM. The later concentration being equivalent to a particle density of the salt ions of $\rho_s = 0.01$.

A homogeneous electric field with reduced field strength $E = 0.1$ is applied in x-direction creating a force $F_{\text{E}} = qE$ on all charged particles, and thus inducing an electrophoretic mobility. It has been carefully checked that the field strength is within the linear response regime, *i.e.*, it does not influence the chain conformation or the distribution of the surrounding ions [11].

Full electrostatic interactions are calculated with the P3M algorithm using the implementation of Reference 15. The Bjerrum length

$$l_{\text{B}} = e_0^2 / (4\pi\epsilon_0\epsilon_r k_{\text{B}}T) = 1.8$$

in simulation units corresponds to 7.1 Å, the Bjerrum length in water at room temperature. This means that the effect of the surrounding water is modelled implicitly by simply using the dielectric properties of water, having a relative dielectric constant of $\epsilon_r \approx 80$.

The simulations are carried out under periodic boundary conditions in a cubic simulation box. The size L of the box is varied to realize a constant monomer concentration of $c_{\text{PE}} = 16$ mM independent of chain length. This is equivalent to a monomer density $\rho_{\text{PE}} = 0.001$.

We include hydrodynamic interactions by using a Lattice Boltzmann algorithm [16] that is interacting with the beads in the MD simulations via a frictionally coupling introduced by Ahlrichs et al. [17]. The mesoscopic LB fluid is described by a velocity field generated by discrete momentum distributions on a spatial grid rather than explicit fluid particles. We use an implementation of the D3Q19 model with a kinematic viscosity $\nu = 1.0$, and a fluid density $\rho = 1.0$. The resulting fluid has a dynamic viscosity $\eta = \rho\nu = 1.0$. The simulation box is discretised by a grid with spacing $a = 1.0$. As usual in a standard Langevin approach, the particle-fluid interaction is realised by a dissipative force. This force depends on the difference between the particle velocity \mathbf{v} and the fluid velocity at the particle position \mathbf{u} :

$$\mathbf{F}_{\text{R}} = -\Gamma_{\text{bare}}(\mathbf{v} - \mathbf{u}).$$

Here, the coupling constant takes on the value $\Gamma_{\text{bare}} = 20.0$. Additional random fluctuations introduced to the particles and fluid act as a thermostat. The interaction between particles and fluid conserve total momentum, and this algorithm has been shown to yield correct long-range hydrodynamic interaction between individual particles [17].

Additionally, a second type of MD simulation is used which is based on the Langevin equations of motions with a velocity dependent dissipative and a random term in addition to the inter particle forces. Together, both additional terms implicitly model the effects of a solvent surrounding the particles: the dissipative force,

$$\mathbf{F}_D = -\Gamma_0 \mathbf{v},$$

with $\Gamma_0 = 1.0$ provides local friction and the non-correlated zero-mean Gaussian random forces,

$$\mathbf{F}_R = \xi(t),$$

mimic thermal kicks (Brownian motion). In order to fulfill the fluctuation-dissipation theorem, dissipative and random force have to be coupled together: $\langle \xi_i(t) \cdot \xi_j(t') \rangle = 6\Gamma_0 k_B T \delta_{ij} \delta(t - t')$. This approach only offers local particle-fluid interactions, and therefore destroys long-range hydrodynamic interactions. Nevertheless one can use it to compute the effective charge as has been presented in [10, 11]. This effective charge is used to obtain the effect friction in the presence of hydrodynamic interactions and illustrates their importance for the electrophoretic mobility.

All simulations are carried out with a MD time step $\tau_{\text{MD}} = 0.01$ and LB time step $\tau_{\text{LB}} = 0.05$. After an equilibration time of 10^6 steps, 10^7 steps are used for generating the data. The time-series of four independent simulations are analyzed using auto-correlation functions to estimate the statistical errors as detailed in Reference 18. Error bars of the order of the symbol size or smaller are omitted in the figures.

3 Results and discussion

3.1 Electrophoretic mobility

We determine the electrophoretic mobility μ as the ratio between the measured center of mass velocity v_{PE} and the magnitude of the electric field E :

$$\mu = \frac{v}{E}.$$

For comparison, the results are normalized by the monomer mobility μ_1 .

Figure 2 displays the characteristic behaviour of flexible polyelectrolytes for vanishing salt concentration $c_s = 0$ mM: initially, the electrophoretic mobility increases with N to reach a maximum at intermediate chain lengths and then slowly decays towards a constant value for long chains. This constant value, often called the free-draining limit μ_{FD} , can be explained by the length independence of the ratio between effective charge and effective friction for long chains as we will show in this article.

In the presence of added salt, the long chain mobility is reduced, which is consistent with the experimentally observed [19] behavior. Furthermore, the shape of the curve is influenced, and the maximum at intermediate chains is suppressed for increased salt concentration. At $c_s = 160$ mM the maximum disappears and the measured mobility

becomes length independent within the resolution of the simulation. A further increase of the added salt concentration leads to a further reduction of the limiting mobility μ_{FD} , not shown here, while the monomer mobility μ_1 remains almost unchanged. This leads eventually to an inverted length-dependence with a monotonic decrease of the mobility towards the limiting value.

In the simple local force picture, the constant center of mass velocity v_{PE} that determines the electrophoretic mobility is a direct result of the cancellation of two acting forces: the electric driving force $F_{\text{E}} = Q_{\text{eff}}E$ is canceled by the solvent friction or drag force $F_{\text{D}} = \Gamma_{\text{eff}}v_{\text{PE}}$. Here, Q_{eff} is the effective charge of the polyelectrolyte, which can be thought of as the bare charge of the polyelectrolyte reduced by oppositely charged ions in solution that associate to the polyelectrolyte chain. The association of counterions to a PE chain is known as counterion condensation [20, 21]. The compound formed by the polyelectrolyte and the associated ions is moved through the solvent under the influence of the external field and experiences a Stokesian drag force with an effective friction coefficient Γ_{eff} that is a priori unknown. In the steady state both forces balance and the mobility is given by

$$\mu = \frac{v}{E} = \frac{Q_{\text{eff}}}{\Gamma_{\text{eff}}}.$$

Next, let us compare the results of Figure 2 to the case when long-range hydrodynamic interactions between the particles are neglected in simulations, *i.e.*, by using a standard Langevin thermostat. The results are shown in Figure 3. One immediately notices that the observed electrophoretic mobility differs significantly from the behaviour observed in Figure 2. Independent of the salt concentration, the mobility decreases monotonically with chain length and slowly approaches a constant value for long chains which is independent of the salt concentration. This difference to the experimental observations and to the LB simulation including hydrodynamics will be analyzed in detail in the following sections.

3.2 Effective charge

To analyze the observed influence of the added salt on the polyelectrolyte mobility, we will determine the effective charge, and can then calculate $\Gamma_{\text{eff}} = Q_{\text{eff}}/\mu$ to obtain an estimate for the effective friction of the polyelectrolyte-ion compound. A word of care has to be taken here, since the value of the effective charge depends on definition. Qualitatively one can differentiate between a static definition and a dynamic definition [22]. In our case it is obviously a dynamic definition. In [10, 11], we introduced several static and dynamic estimators for the effective charge and showed their equivalence at vanishing salt concentration. Here, three of them will be reviewed and applied to the case of added salt.

The local force picture described above can be used to estimate the effective charge of the polyelectrolyte based on the measurement of the electrophoretic mobility in the absence of hydrodynamic interactions. Let N_{CI} be the number of associated counterions reducing the bare charge of the polyelectrolyte which is equal to N . The effective charge is then given by

$$Q_{\text{eff}} = N - N_{\text{CI}}.$$

Without long-rang hydrodynamic interactions the interaction of each particle with the solvent is purely local and directly given by the friction constant Γ_0 of the Langevin

algorithm. The total effective friction of the polyelectrolyte and the ions is then:

$$\Gamma_{\text{eff}} = \Gamma_0 (N + N_{\text{CI}}).$$

This results in an expression for the electrophoretic mobility

$$\mu = \frac{N - N_{\text{CI}}}{\Gamma_0 (N + N_{\text{CI}})}$$

from which an expression for N_{CI} is obtained. Therefore we can express the effective charge purely as a function of the mobility measurements shown in Figure 3 and on our input value for Γ_0 , independent of the knowledge of the value of $N_c l$ by the following expression:

$$Q_{\text{eff}}^{(1)} = N \left(1 - \frac{1 - \mu \Gamma_0}{1 + \mu \Gamma_0} \right).$$

An alternative way of characterizing the associated ions is presented in Ref. 23 who suggested to determine the ion velocity with respect to the distance to the center of mass of the polyelectrolyte. For this method we use the LB algorithm to include hydrodynamical interactions, and the result for a chain of $N = 64$ at $c_s = 16$ mM can be inspected in Figure 4. The average ion velocity in the direction of the electric field v_{CI} is a function of the distance d to the center of mass of the polyelectrolyte chain and in general depends on the chain length N and the salt concentration c_s . As shown, ions close to the center move with the chain at negative speed, whereas ions far away from the center move with the single particle velocity $v_1 = \mu_1 E$ into the opposite direction. The association of ions to the chain is strong enough to move them against the electric field. For every chain length and every salt concentration, the distance d_0 at which $v_{\text{CI}}(d_0) = 0$ is used to separate co-moving, associated ions from non-associated ones.

We use this distance d_0 to define the effective charge by summing up the total charge in the system found within this distance to the center of mass of the polyelectrolyte:

$$Q_{\text{eff}}^{(2)} = N (1 - I(d_0)),$$

where $I(d_0)$ is the integrated fraction of neutralizing charges found by adding the number of counterions and positively charged salt ions reduced by the number of negatively or like-charged salt ions. Far away from the center of mass of the chain, the total bare charge of the polyelectrolyte is neutralized and $I = 1$.

The effective charge Q_{eff} as obtained from both estimators is presented in Figure 5a. Initially, Q_{eff} is close to the bare charge N , but as ion condensation sets in, the effective charge is reduced. Longer chains show a linear increase of their charge close to the Manning prediction for counterion condensation in the salt free case $Q_{\text{eff}} = (1/\xi) N$, where Manning parameter $\xi = l_B/b$ is the ratio between the Bjerrum length and the charge spacing along the polyelectrolyte backbone. For the model used here $b = 0.9$ and therefore $\xi = 2.0$. We note that there is no apparent dependence of the effective charge for long polyelectrolyte chains on the salt concentrations when measured by the dynamic effective charge estimators presented here.

Figure 5b plots the effective charge per monomer, Q_{eff}/N . Here, the influence of the salt concentration for short and intermediate chain length can be seen. The higher the concentration of the added salt, the faster the electric charge of the polyelectrolyte is reduced by condensed counter ions. For long chains, the charge per monomer is again independent of the salt concentration and comparable to the Manning prediction $1/\xi$.

The difference for short and intermediate chains at different salt concentrations can be attributed to stronger association of counterions with increasing salt concentrations. For short chains, smaller than the Debye length, effects due to the finite size play a leading role in the ability to condense counterions [24, 25, 26].

Additionally, Figure 5 shows the equivalence of the two dynamic estimators $Q_{\text{eff}}^{(1)}$ and $Q_{\text{eff}}^{(2)}$ independently of the presence or absence of hydrodynamic interactions also in the presence of additional salt. This new observation supports the applicability and importance of these charge estimators for the study of polyelectrolytes during electrophoresis.

The charge estimators $Q_{\text{eff}}^{(1)}$ and $Q_{\text{eff}}^{(2)}$ measure the effective charge of the moving polyelectrolyte and its surrounding counterions. Therefore, they measure the effective dynamic charge of the polyelectrolyte. Similarly, it is possible to define a static estimate of the effective charge using the following simple method

$$Q_{\text{eff}}^{(3)} = N_{\text{PE}} - N_{\text{CI}}(d < d_0),$$

where $N_{\text{CI}}(d < d_0)$ is the average number of counterions that can be found within a distance d to the closest monomer. Here, the threshold d_0 chosen to be $d_0 = 2\sigma_0$.

The second static charge estimator used in Ref. 11 based on the inflection criterion to estimate the threshold of counterion condensation [27, 28, 29] breaks down in the presence of high salt concentrations and therefore can not be applied here.

In Figure 6, we compare the static charge estimate $Q_{\text{eff}}^{(3)}$ for varying salt concentrations to the dynamic charge estimate obtained by $Q_{\text{eff}}^{(1)}$. Unlike the dynamic estimate the static charge estimate shows a strong dependence on the salt concentration. While both estimators agree for vanishing salt concentration as previously shown in Ref. 11, the static charge estimate shows a decrease with higher salt concentrations, hence an increase in counterion condensation, as could be expected from a mean-field comparison [29], and eventually falls below the Manning prediction.

The higher salt concentrations increase the number of counterions in the close vicinity of the chain as measured by $Q_{\text{eff}}^{(3)}$. At the same time, the electrostatic interactions in the system are reduced due to electrostatic screening, which also reduces the strength of the coupling between the polyelectrolyte and the counterions. The independence of the dynamic effective charge on the salt concentration for long chains as shown in Figure 5 has to be understood as the cancellation of both effects: with increasing salt concentration more counterions in close vicinity to the polyelectrolyte are influenced by the chain but the strength of the interactions is reduced in such a way that the combined action remains unchanged and yields a concentration independent dynamic effective charge.

In the following, we will use the dynamic effective charge to calculate the effective friction of the polyelectrolyte-ion compound.

3.3 Effective friction

When long-range hydrodynamic interactions are present, the effective friction of the polyelectrolyte and the associated counterions cannot be given in a simple analytic form. We therefore obtain it from the measurements of the mobility and the effective charge presented above:

$$\Gamma_{\text{eff}} = \frac{Q_{\text{eff}}}{\mu}.$$

In Figure 7a, the effective charge Γ_{eff} is displayed as a function of chain length N for different salt concentrations c_s . The friction increases monotonically with chain length.

Neglecting the contribution of the counterions the effective friction can be obtained from the hydrodynamic radius R_h of the polyelectrolyte defined by:

$$\left\langle \frac{1}{R_h} \right\rangle = \frac{1}{N} \sum_{i \neq j} \left\langle \frac{1}{\|\vec{r}_i - \vec{r}_j\|} \right\rangle.$$

Here, \vec{r}_i is the position of the i -th chain monomer, and \vec{r}_{cm} the center of mass of the polyelectrolyte chain. The angular brackets $\langle \dots \rangle$ indicate an ensemble average. The hydrodynamic radius is expected to exhibit a power law scaling $R_h \sim (N - 1)^\nu$, where the scaling exponent ν depends on the system. For an uncharged polymer with ideal chain behaviour one should get $\nu \approx 0.588$ (Flory exponent) [30], whereas for a fully charged polyelectrolyte without electrostatic screening one expects $\nu = 1$. Depending on the salt concentration, we obtain values between $\nu \approx 0.66$ for $c_s = 0$ mM and $\nu \approx 0.59$ for $c_s = 160$ mM (not shown here).

Initially, the friction increases with N as given by the hydrodynamic size of the polyelectrolyte

$$\Gamma = 6\pi\eta R_h \propto N^{0.61}.$$

With the onset of counterion condensation the friction exceeds the value of the bare polyelectrolyte and for long chains becomes linear in N . The higher the concentration of the additional salt, the earlier the transition between the two regimes is observed. We furthermore note that the absolute friction value is increased with the addition of external salt.

The role of the additional salt can be best understood when looking at the effective friction per monomer as presented in Figure 7b. Γ_{eff}/N shows an initial decrease with chain length which can be understood by hydrodynamic shielding: the monomers of short polyelectrolyte chains are hydrodynamically coupled and shield each other from the effect of the solvent. This reduces the friction per monomer below the value of a single particle. The decrease in friction due to the hydrodynamic shielding is stronger the lower the salt concentration is. The presence of ions in the vicinity of the chain monomers reduces the hydrodynamic coupling. For longer length scale, *i.e.*, for longer chains, the ions effectively decouple different parts of the polyelectrolyte chain such that the friction per monomer becomes a constant value. The chain length N_{FD} for which this transition occurs is depending on the salt concentration. The higher the salt concentration, *i.e.*, the shorter the Debye length in the system, the more confined is the hydrodynamic shielding effect and the earlier the effective friction becomes constant.

The role of hydrodynamic interactions for the effective friction of the polyelectrolyte can be seen by comparing Figure 7 to Figure 8 that shows the effective friction obtained with the Langevin algorithm neglecting long-range hydrodynamic interactions. In Figure 8a, the initial increase of the effective friction is super linear, but linear scaling is reached for longer chains. The absolute friction value for long chains is independent of the salt concentration. This can be understood by realizing that the total effective friction of a polyelectrolyte in the Langevin algorithm is only based on the local friction parameter Γ_0 and the number of co-moving particles, *i.e.*, the sum of N monomers and N_{CI} condensed counterions: $\Gamma_{\text{eff}} = \Gamma_0 (N + N_{\text{CI}})$. As shown in Figure 5 the effective charge, and therefore also N_{CI} and Γ_{eff} , is only influenced by the salt concentration for

short and intermediate chains, but not for long chains. Figure 8b shows the increase of the effective friction per monomer from $\Gamma_{\text{eff}}(1) = 1/\mu_1 \approx \Gamma_0$ to a constant value for long chains, which is comparable to the plateau value predicted using counterion condensation theory: $\Gamma_{\text{eff}}/N = \Gamma_0(2 - 1/\xi)$.

Figure 9 schematically illustrates how counterions and salt in the vicinity of polyelectrolyte chains influence the hydrodynamic interactions during electrophoresis. Figure 9a indicates the regime, where all parts of the chain can interact via hydrodynamic interactions. The individual chain segments provide hydrodynamic shielding to each other. During electrophoresis, see Figure 9, the counterions within the polyelectrolyte limit the range of the hydrodynamic interaction. The hydrodynamic screening length depends on the ion concentration in the vicinity of the chain. This relation between the ion density and the hydrodynamic screening length was previously suggested by different authors [31, 32].

The connection between electrostatic screening and hydrodynamic screening can be easily motivated by the following reasoning: the Debye length is the length-scale on which the charge of the polyelectrolyte is screened by the surrounding ions. When looking at this object from the outside, the total force exerted by the applied electric field is zero, *i.e.*, no momentum is transferred to the polyelectrolyte-ion complex. Due to momentum conservation, the interaction with the fluid has to result in a vanishing total force.

The counterions that associate with the polyelectrolyte influence the solvent flow around it, effectively canceling the beneficial shielding effects. When additional salt is added to the system, the like charged salt ions likewise contribute to this effect as shown in Figure 9c. The higher the ion concentration is, *i.e.*, the shorter the Debye length is, the shorter is the length scale on which different polyelectrolyte monomers can interact hydrodynamically. On a length scale comparable to the Debye length in the system, different parts of the polyelectrolyte become decoupled. For longer chains, the effective friction per segment does not depend on the length of the polyelectrolyte anymore. Consequently, the effective friction per monomer becomes independent of the length of the polyelectrolyte chain, as seen in Figure 7b.

4 Conclusion

We presented a detailed study of the electrophoretic behaviour of flexible polyelectrolyte chains by means of a mesoscopic coarse-grained molecular dynamics model including full hydrodynamic and electrostatic interactions.

The electrophoretic mobility exhibits a characteristic length dependence for short polyelectrolyte chains and a constant length independent value for long chains. We showed that both, the shape and the constant long chain value, depend on the salt concentration of the solution if hydrodynamical interactions were properly accounted for. The long chain mobility was then found to be decreasing with increasing salt concentration, in agreement with experimental observations.

Direct measurements of the effective charge by two independent estimators showed that the dynamic effective charge for long chains is independent of the salt concentration. We therefore conclude, that the dependence of the long chain mobility on the salt concentration is not due a reduced effective charge but has to be attributed to a change in the effective friction. On the other hand, the effective charge for short and intermediate chains is influenced by the salt concentration which explains the different

behaviour of the electrophoretic mobility in this regime.

We note that a static estimate of the effective charge shows a dependence on the salt concentration leading to different charge estimates for finite salt concentrations: a static and a dynamic effective charge.

We showed that the effective friction of the polyelectrolyte is strongly influenced by the presence of ions in the solution. For short chains and low salt concentrations no counterions are associated with the polyelectrolyte chain and the effective friction is given by the hydrodynamic radius. The presence of ions in the vicinity of the chain reduces the hydrodynamic shielding between the chain monomers and leads to an increased friction. The longer the chains and the higher the salt concentration, the more the shielding is reduced, until for chains longer than a specific length N_{FD} the friction becomes linear with chain length. In this regime, different parts of the chain are effectively decoupled.

From this, the specific behaviour of the electrophoretic mobility as observed in experiments can be understood: the hydrodynamic shielding between the monomers allows for an initial increase in the mobility. The onset of counterion condensation counteracts this increase as it reduces the effective charge and at the same time increases the effective friction. For long chains, charge and friction both become linearly dependent on chain length which therefore results in the well-known constant mobility, or free-draining limit.

The presence of salt reduces the length scale on which the chain monomers can interact hydrodynamically. This reduces the initial hydrodynamic shielding and therefore suppresses the mobility maximum. At the same time, the total friction is increased leading to a reduced long-chain mobility. Salt concentrations exceeding the ones in this simulation can cause a total decoupling of the individual chain monomers, which can then be simulated without hydrodynamic interactions. We expect a length-dependence of the mobility as shown in Figure 3 and an effective friction per monomer, *cf.* Figure 7b, that does not depend on N .

The study shows that chemical details and fluid structure can be neglected, and a higher level of abstraction yields an accurate description of the physics of the problem, as long as electrostatic and hydrodynamic interactions between all entities in the system, i.e., the polyelectrolyte, dissociated counterions, additional salt and the solvent, are properly accounted for. In this way we were able to model a process bridging the single molecule regime of a few nm up to macromolecules with contour lengths of more than 100 nm, a regime currently not accessible to atomistic simulations.

Acknowledgements

Funds from the the Volkswagen foundation, the DAAD, and DFG under the TR6 are gratefully acknowledged. All simulations were carried out on the compute cluster of the Center for Scientific Computing (CSC) at Goethe University Frankfurt/Main.

References

- [1] ed. P. G. Righetti, *Capillary Electrophoresis in Analytical Biotechnology*, CRC Press, Boca Raton, 1996.
- [2] V. Dolnik, January , 2006, **27**(1), 126–141.
- [3] H. Cottet, C. Simo, W. Vayaboury, and A. Cifuentes, March , 2005, **1068**(1), 59–73.
- [4] H. Cottet and P. Gareil, Humana Press, NJ, USA, 2007; chapter Separation of synthetic (co)polymers by capillary electrophoresis techniques.
- [5] J.-L. Barrat and J.-F. Joanny, *Advances in Chemical Physics*, 1996, **94**, 1–66.
- [6] M. Muthukumar, June , 1996, **17**(6), 1167–1172.
- [7] A. R. Volkel and J. Noolandi, April , 1995, **102**(13), 5506–5511.
- [8] U. Mohanty and N. C. Stellwagen, March , 1999, **49**(3), 209–214.
- [9] K. Grass, U. Böhme, U. Scheler, H. Cottet, and C. Holm, *Physical Review Letters*, 2008, **100**, 096104.
- [10] K. Grass and C. Holm, *J. Phys.: Condens. Matter*, 2008, **20**(494217).
- [11] K. Grass and C. Holm, *Submitted.*, 2008.
- [12] H. J. Limbach, A. Arnold, B. A. Mann, and C. Holm, May , 2006, **174**(9), 704–727.
- [13] T. Soddemann, B. Dünweg, and K. Kremer, *Eur. Phys. J. E*, 2001, **6**, 409.
- [14] J. D. Weeks, D. Chandler, and H. C. Andersen, *J. Chem. Phys.*, 1971, **54**, 5237.
- [15] M. Deserno and C. Holm, *J. Chem. Phys.*, 1998, **109**, 7678.
- [16] G. R. McNamara and G. Zanetti, NOV 14 , 1988, **61**(20), 2332–2335.
- [17] P. Ahlrichs and B. Dünweg, *J. Chem. Phys.*, 1999, **111**(17), 8225–8239.
- [18] U. Wolff, *Comput. Phys. Commun.*, 2004, **156**, 143–153.
- [19] D. A. Hoagland, E. Arvanitidou, and C. Welch, September , 1999, **32**(19), 6180–6190.
- [20] G. Manning, *J. Chem. Phys.*, 1969, **51**, 924–933.
- [21] F. Oosawa, *Polyelectrolytes*, Marcel Dekker, New York, 1971.
- [22] P. Wette, H. Schöpe, and T. Palberg, *J. Chem. Phys.*, 2002, **116**, 10981.
- [23] V. Lobaskin, B. Dünweg, and C. Holm, sep , 2004, **16**(38), S4063–S4073.
- [24] H. J. Limbach and C. Holm, *J. Chem. Phys.*, 2001, **114**(21), 9674–9682.
- [25] D. Antypov and C. Holm, *Phys. Rev. Lett.*, 2006, **96**, 088302.

- [26] D. Antypov and C. Holm, *Macromolecules*, 2007, **40**(3), 731–738.
- [27] L. Belloni, M. Drifford, and P. Turq, *Chem. Phys.*, 1984, **83**, 147.
- [28] L. Belloni, *Colloids and Surfaces*, 1998, **A 140**, 227.
- [29] M. Deserno, C. Holm, and S. May, *Macromolecules*, 2000, **33**, 199–206.
- [30] M. A. Moore and A. J. Bray, *Journal of Physics A-Mathematical and General*, 1978, **11**(7), 1353–1359.
- [31] D. Long and A. Ajdari, January , 2001, **4**(1), 29–32.
- [32] M. Tanaka and A. Y. Grosberg, *J. Chem. Phys.*, 2001, **115**(1), 567–574.

- Fig. 1** The normalized electrophoretic mobility μ/μ_{FD} as a function of the number of repeat units N for simulation data including hydrodynamic interactions (HI), and experimental data coming from capillary electrophoresis (CE) and from electrophoretic NMR. The inset compares to simulation data obtained with a model neglecting hydrodynamic interactions.
- Fig. 2** The normalized electrophoretic mobility μ/μ_1 of polyelectrolyte chains of length N for three different salt concentrations using the LB algorithm. The added salt not only influences the absolute mobility, but likewise changes the characteristic shape of the mobility with respect to chain length N .
- Fig. 3** The normalized electrophoretic mobility μ/μ_1 for different chain length N at varying salt concentrations c_s without hydrodynamic interactions differs significantly from the behaviour observed in Figure 2. The mobility shows a salt-dependent monotonic decrease for short chains and a salt-independent constant value for long chains.
- Fig. 4** The average ion velocity in the direction of the electric field v_{CI} (here for a chain with $N = 64$ monomers, salt concentration $c_s = 16$ mM, and hydrodynamics included) depends on the distance d to the center of mass of the polyelectrolyte. Ions close to the center co-move with the chain's velocity (dashed line), whereas ions far away from the center move with the single particle velocity $v_1 = \mu_1 E$ into the opposite direction. The distance d_0 at which $v_{\text{CI}}(d_0) = 0$ is used to separate co-moving, associated ions from non-associated ones. The solid line shows the integrated fraction of charges I that is found up to the distance d of the center of mass.
- Fig. 5** (a) The effective charge Q_{eff} as a function of chain length N (symbols for $Q_{\text{eff}}^{(1)}$, lines for $Q_{\text{eff}}^{(2)}$). Both charge estimators show good agreement. Initially, Q_{eff} is close to the bare charge N (dotted line), but as ion condensation sets in, the effective charge is reduced. Longer chains show a linear increase of their charge close to the Manning prediction $(1/\xi)N$ (dashed line). (b) The effective charge per monomer $Q_{\text{eff}/N}$ is influenced by the salt concentration for short and intermediate chains. The higher the concentration of the added salt, the faster the electric charge of the polyelectrolyte is reduced by condensed ions. For long chains, the charge per monomer is again independent of the salt concentration and comparable to the Manning prediction $1/\xi$ (dashed line).
- Fig. 6** The effective charge as measured by the static estimator $Q_{\text{eff}}^{(3)}$ shows a strong dependence on the the salt concentration. At $c_s = 0$ mM the static estimate agrees with the dynamic estimates (solid line). The higher the salt concentration, the lower is the static charge estimate. For comparison the bare charge N (dotted line) and the Manning prediction (dashed-line) are plotted.

Fig. 7 (a) The normalized effective friction $\Gamma_{\text{eff}}\mu_1$ as a function of chain length N for different salt concentrations c_s using the LB algorithm. Initially, the friction increases as given by the hydrodynamic size of the polyelectrolyte $\Gamma \sim N^{0.59}$ (dotted line). With the onset of counterion condensation the friction exceeds the value of the bare polyelectrolyte and for long chains becomes linear in N (dashed line). The absolute friction value is increased with the addition of external salt. (b) The normalized effective friction per monomer $\Gamma_{\text{eff}}\mu_1/N$ shows an initial decrease with chain length that is stronger the lower the salt concentration is. From a concentration dependent value of N_{FD} onwards, the friction per monomer becomes a constant value that increases with increasing salt concentration (indicated by dashed lines).

Fig. 8 (a) The normalized effective friction $\Gamma_{\text{eff}}\mu_1$ as a function of chain length N for different salt concentrations c_s without long-range hydrodynamic interactions. Initially, the increase of the effective friction is super linear, but linear scaling (dotted line) is reached for longer chains. For these chains, the absolute friction value is independent of the addition of external salt. (b) The normalized effective friction per monomer $\Gamma_{\text{eff}}\mu_1/N$ shows an initial increase with chain length that is stronger the higher the salt concentration is. For longer chains, a plateau value is reached which is independent of the salt concentration and can be compared to the predicted value based on the counterion condensation theory (dashed line).

Fig. 9 Illustration of the influence of surrounding ions on to the long-range hydrodynamic interactions between different parts of a polyelectrolyte chain. (a) For an uncharged polymer, the hydrodynamic interactions are unscreened and all chain monomers can interact with each other. (b) The presence of counterions during electrophoresis of polyelectrolytes limits the hydrodynamic interaction. (c) The more salt is added to the system, the higher is the ion density in the vicinity of the chain, which reduces the hydrodynamic interaction range even further, so that most parts of the chain appear to be hydrodynamically decoupled.

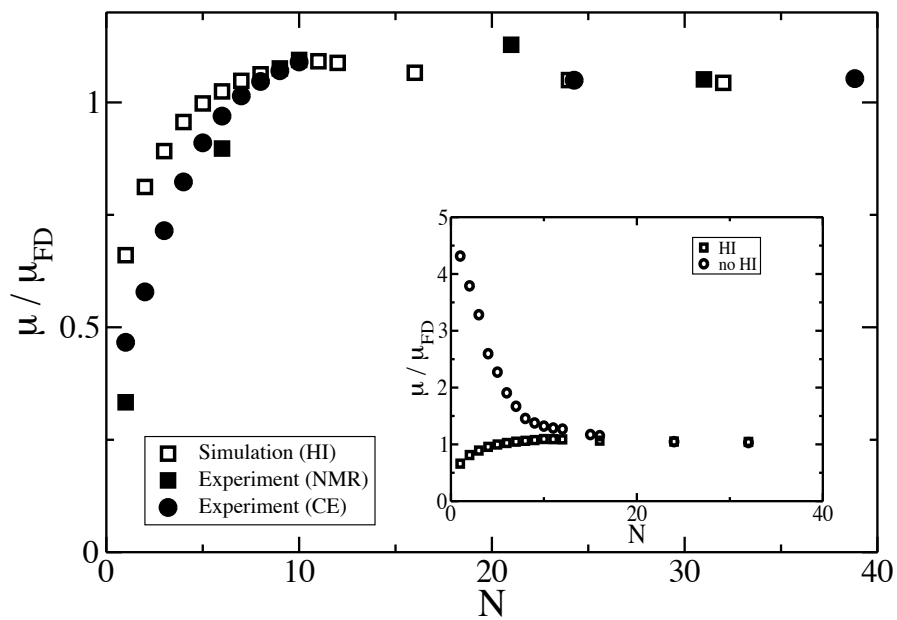


Figure 1: The normalized electrophoretic mobility μ/μ_{FD} as a function of the number of repeat units N for simulation data including hydrodynamic interactions (HI), and experimental data coming from capillary electrophoresis (CE) and from electrophoretic NMR. The inset compares to simulation data obtained with a model neglecting hydrodynamic interactions.

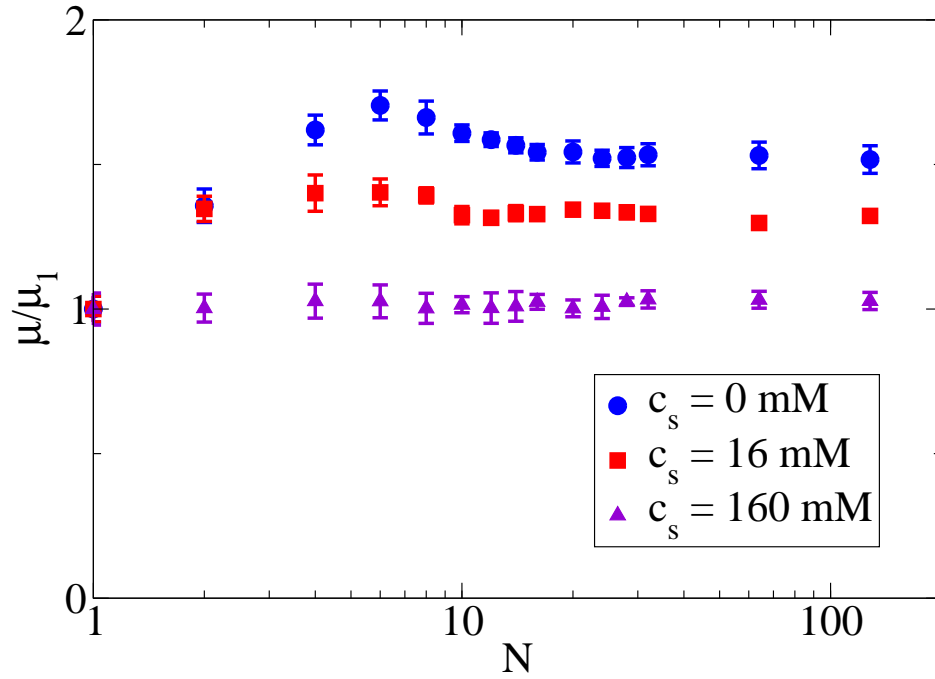


Figure 2: The normalized electrophoretic mobility μ/μ_1 of polyelectrolyte chains of length N for three different salt concentrations using the LB algorithm. The added salt not only influences the absolute mobility, but likewise changes the characteristic shape of the mobility with respect to chain length N .

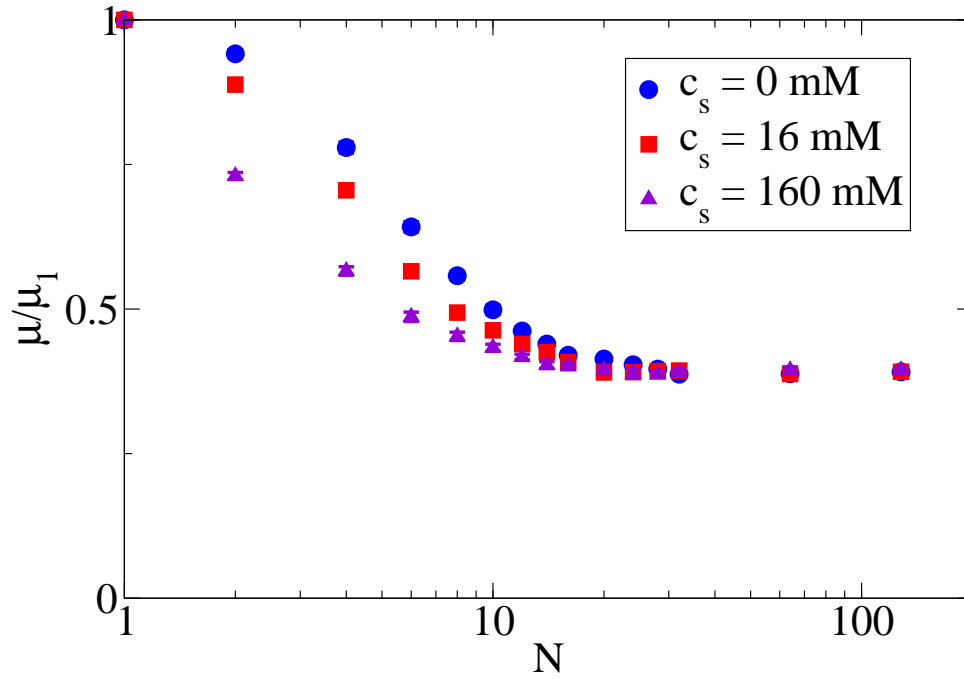


Figure 3: The normalized electrophoretic mobility μ/μ_1 for different chain length N at varying salt concentrations c_s without hydrodynamic interactions differs significantly from the behaviour observed in Figure 2. The mobility shows a salt-dependent monotonic decrease for short chains and a salt-independent constant value for long chains.

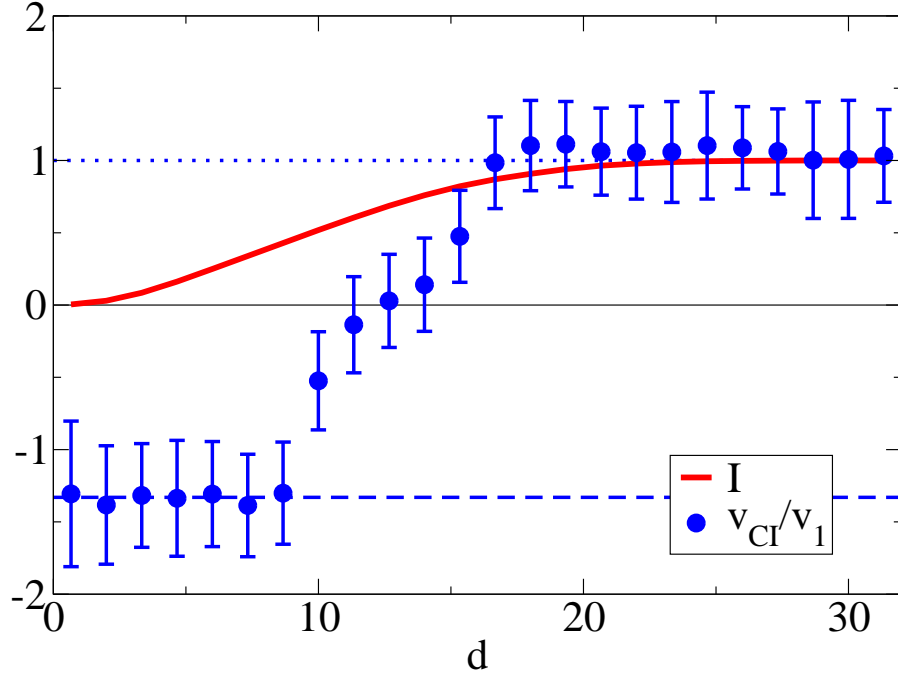


Figure 4: The average ion velocity in the direction of the electric field v_{CI} (here for a chain with $N = 64$ monomers, salt concentration $c_s = 16$ mM, and hydrodynamics included) depends on the distance d to the center of mass of the polyelectrolyte. Ions close to the center co-move with the chain's velocity (dashed line), whereas ions far away from the center move with the single particle velocity $v_1 = \mu_1 E$ into the opposite direction. The distance d_0 at which $v_{CI}(d_0) = 0$ is used to separate co-moving, associated ions from non-associated ones. The solid line shows the integrated fraction of charges I that is found up to the distance d of the center of mass.

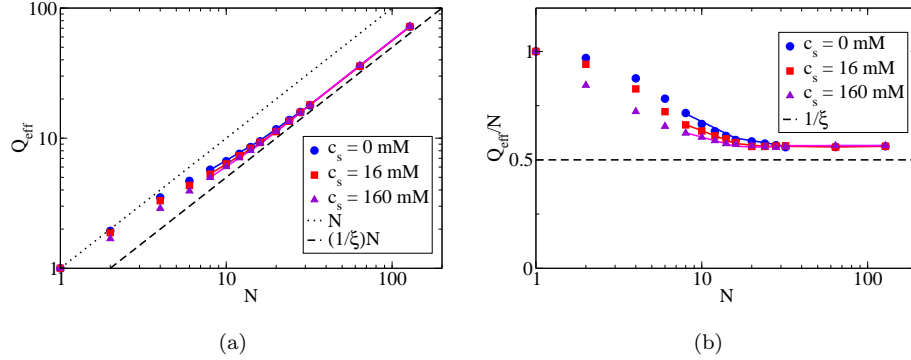


Figure 5: (a) The effective charge Q_{eff} as a function of chain length N (symbols for $Q_{\text{eff}}^{(1)}$, lines for $Q_{\text{eff}}^{(2)}$). Both charge estimators show good agreement. Initially, Q_{eff} is close to the bare charge N (dotted line), but as ion condensation sets in, the effective charge is reduced. Longer chains show a linear increase of their charge close to the Manning prediction $(1/\xi)N$ (dashed line). (b) The effective charge per monomer Q_{eff}/N is influenced by the salt concentration for short and intermediate chains. The higher the concentration of the added salt, the faster the electric charge of the polyelectrolyte is reduced by condensed ions. For long chains, the charge per monomer is again independent of the salt concentration and comparable to the Manning prediction $1/\xi$ (dashed line).

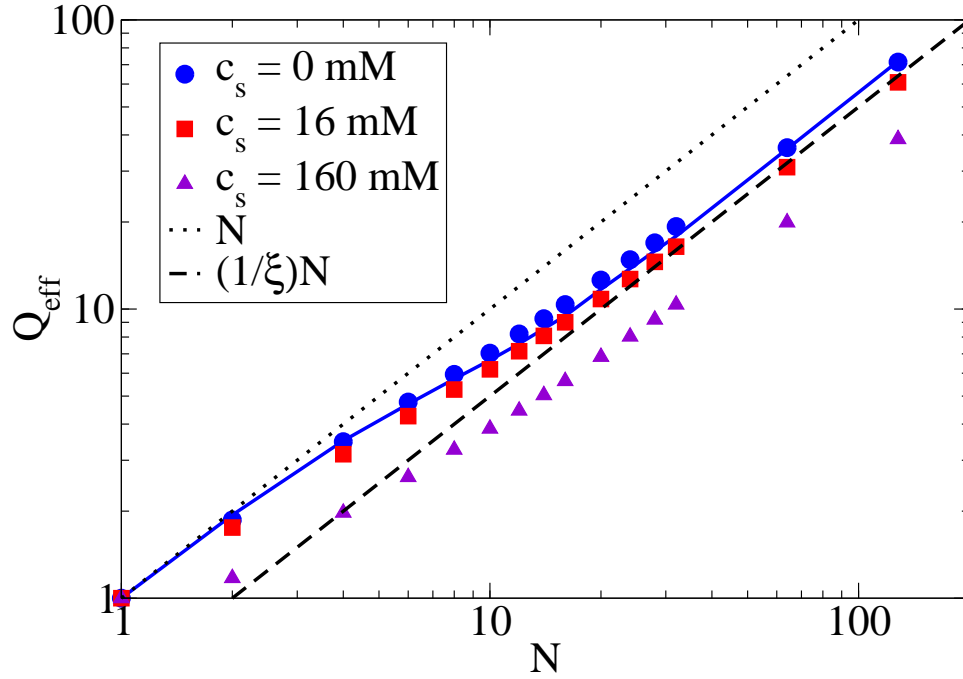


Figure 6: The effective charge as measured by the static estimator $Q_{\text{eff}}^{(3)}$ shows a strong dependence on the the salt concentration. At $c_s = 0$ mM the static estimate agrees with the dynamic estimates (solid line). The higher the salt concentration, the lower is the static charge estimate. For comparison the bare charge N (dotted line) and the Manning prediction (dashed-line) are plotted.

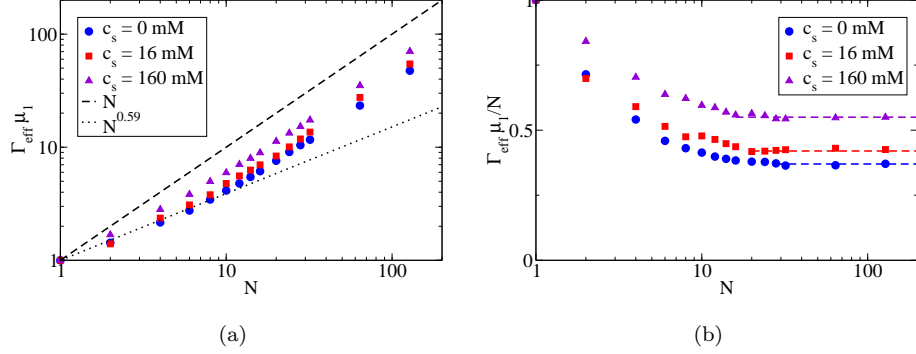


Figure 7: (a) The normalized effective friction $\Gamma_{\text{eff}}\mu_1$ as a function of chain length N for different salt concentrations c_s using the LB algorithm. Initially, the friction increases as given by the hydrodynamic size of the polyelectrolyte $\Gamma \sim N^{0.59}$ (dotted line). With the onset of counterion condensation the friction exceeds the value of the bare polyelectrolyte and for long chains becomes linear in N (dashed line). The absolute friction value is increased with the addition of external salt. (b) The normalized effective friction per monomer $\Gamma_{\text{eff}}\mu_1/N$ shows an initial decrease with chain length that is stronger the lower the salt concentration is. From a concentration dependent value of N_{FD} onwards, the friction per monomer becomes a constant value that increases with increasing salt concentration (indicated by dashed lines).

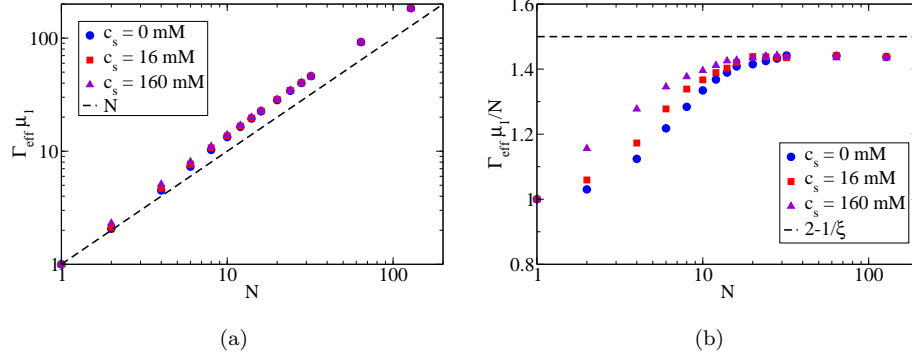


Figure 8: (a) The normalized effective friction $\Gamma_{\text{eff}} \mu_1$ as a function of chain length N for different salt concentrations c_s without long-range hydrodynamic interactions. Initially, the increase of the effective friction is super linear, but linear scaling (dotted line) is reached for longer chains. For these chains, the absolute friction value is independent of the addition of external salt. (b) The normalized effective friction per monomer $\Gamma_{\text{eff}} \mu_1 / N$ shows an initial increase with chain length that is stronger the higher the salt concentration is. For longer chains, a plateau value is reached which is independent of the salt concentration and can be compared to the predicted value based on the counterion condensation theory (dashed line).

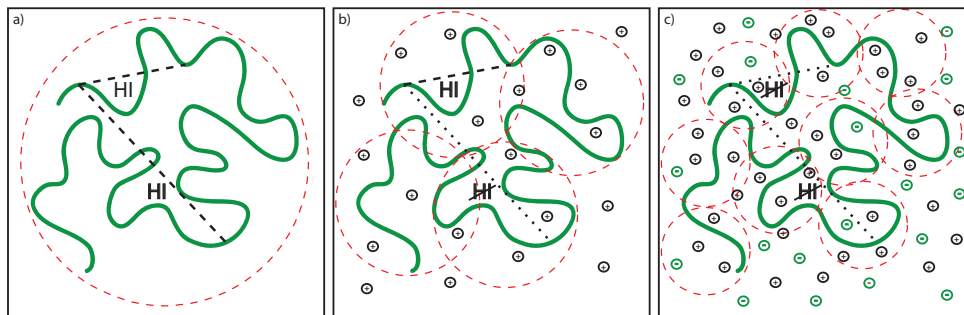


Figure 9: Illustration of the influence of surrounding ions on to the long-range hydrodynamic interactions between different parts of a polyelectrolyte chain. (a) For an uncharged polymer, the hydrodynamic interactions are unscreened and all chain monomers can interact with each other. (b) The presence of counterions during electrophoresis of polyelectrolytes limits the hydrodynamic interaction. (c) The more salt is added to the system, the higher is the ion density in the vicinity of the chain, which reduces the hydrodynamic interaction range even further, so that most parts of the chain appear to be hydrodynamically decoupled.